Supporting information

Near-Unity MIM Absorber for Thermoelectric Energy Harvesting in Space Environments

Mikita Marus,[a,b] Nikolay Lyapunov,[a] Aliaksandr Hubarevich,[b,c] Remo Proietti Zaccaria,*[b] and Shu-Jen Wang*[a]

[a]*Department of Physics, Hong Kong Baptist University, Kowloon Tong, Kowloon, Hong Kong*
Email: shu-jenwang@hkbu.edu.hk
[b]*Istituto Italiano di Tecnologia, Via Morego 30, I-16163 Genova, Italy*
Email: remo.proietti@iit.it
[c]*Belarusian State University of Informatics and Radioelectronics, 6 P. Brouki, Minsk 220013, Belarus*

Fabrication tolerance and process window

The nanosquare photonic metamaterial (NS-PtMM) is expected to reduce sensitivity to perturbations in geometric parameters (resonator width, pitch, and thickness) compared with the multi-arm nanocross PtMM (NC-PtMM). This is because a single geometric length scale dominates the square resonance and supports fewer closely spaced resonant modes; consequently, a ±10% variation in lateral dimensions primarily shifts the spectral position without significantly degrading the integrated absorptance. In contrast, the nanocross relies on interference between orthogonal arms and multiple coupling channels, increasing susceptibility to process variation and overlay errors. The square design, therefore, tolerates standard process variability (deposition non-uniformity, line-edge roughness, etch bias) more readily and shows better large-area reproducibility when implemented with nanoimprint or contact photomasks (Table S1), which are desirable manufacturing routes for aerospace surface coatings and panel-level integration[1–4].

Table S1. Comparison of NC-PtMM (performance) vs NS-PtMM (simple/tile)

Metric / Consideration	NC-PtMM (performance)	NS-PtMM (simple/tile)
Peak A_{vis} (%)	High (≈99% peak)	Moderate (≈68–78%)
Broadband $A_{integrated}$ (AM0)	High	Moderate
Fabrication complexity	High – multi-orientation features, tight CD control	Low – single-orientation, single CD
Patterning methods suitable	E-beam, high-resolution NIL, advanced lithography	Photolithography, nanoimprint, soft lithography, maskless stamping
Process tolerance to ±10% CD errors	Lower (spectral shape sensitive)	Higher (spectral shift but preserved integrated absorptance)
Large-area scalability / throughput	Challenging; E-beam costly	Amenable to roll-to-roll/NIL and wafer-scale masks

Yield and uniformity	Lower (sensitive to overlay/roughness)	Higher (robust to local defects)
Thermal hot-spot concentration	High (localized maxima)	Lower (more uniform heating)
Long-term reliability risk (thermal cycling & hotspots)	Higher local stress risk	Lower local stress risk
Integration complexity with the TEG module	Moderate (requires precise thermal interface)	Lower (more uniform contact, simpler bonding)
Suitability for low-cost flight demonstration	Lower (higher risk/cost)	Higher (reduced qualification risk)

Space-qualification test matrix

The PtMM flight qualification plan focuses on environmental stressors relevant to the intended orbit and mission lifetime. Recommended screening tests are: atomic-oxygen (AO) exposure to simulate LEO erosion[5,6], thermal vacuum cycling (TVAC) across mission temperature extremes[7,8], high-flux UV/VUV exposure to assess photochemical degradation[8–10], proton/electron irradiation (TID and displacement damage) to detect optical constant drift[11–13], sputter-yield and erosion tests under ion bombardment[14–16], adhesion and outgassing tests (ASTM E595 compliance)[17], and mechanical vibration/shock[18–20]. For each test, we recommend pre- and post-test optical (R(λ), T(λ), A(λ)), SEM/AFM morphology, optical constants (ellipsometry), mass loss, and electrical contact/resistance check where relevant. Test levels (energies, fluences, and cycle counts) should be chosen per mission orbital parameters and agency standards.

Table S2. Condensed Space-qualification test matrix

Test	Purpose	Typical conditions	Measured outputs
Atomic oxygen (AO)[5,6]	Erosion of exposed films (LEO)	AO fluence scaled to mission; RF AO beam exposure	$\Delta A(\lambda)$, mass loss, SEM roughness
Thermal vacuum cycling (TVAC)[7,8]	Thermal fatigue / adhesion	−100 °C → +120 °C, 100–1000 cycles (mission dependent)	$\Delta A(\lambda)$, delamination, SEM cracks
UV/VUV[8–10]	Photochemical degradation	115–400 nm exposure, mission-equivalent dose	$\Delta A(\lambda)$, color change, optical constants
Proton/electron irradiation (TID)[11–13]	Displacement & ionizing damage	Proton/electron energies & fluences typical for orbit	$\Delta A(\lambda)$, ellipsometry k/n change, SEM

Ion sputter / erosion[14–16]	Material loss under ion flux	Ion species/energy from mission environment	sputter yield (mg/cm^2), $\Delta A(\lambda)$
Adhesion / outgassing[17]	Mechanical integrity & cleanliness	ASTM E595 (TML, CVCM) & tape/peel tests	TML/CVCM, adhesion grade, SEM
Vibration & shock[18–20]	Launch survivability	Random vibration and shock per launcher profile	$\Delta A(\lambda)$, visual / SEM inspection

Feasibility of the NC-PtMM geometry in terms of actual fabrication approach

To test the feasibility of the NC-PtMM geometry in terms of the actual fabrication approach, we exploited the Nanofabrication Facility at the Italian Institute of Technology (IIT). The fabrication method was based on an electron beam (e-beam) lithography. The process was carried out on CaF_2 (100) substrates spin-coated at 1,800 r.p.m. with poly(methyl methacrylate) (MicroChem 950 PMMA A2) electronic resist. An Al film of 10 nm thickness was thermally deposited onto the PMMA surface to avoid charging and drifting effects. Then, an e-beam lithography machine (Raith 150-two) equipped with a pattern generator was used to write the nanostructure directly (electron energy of 20 keV and beam current of 28 pA). After aluminium removal in KOH-H_2O solution (concentration of 1 M), the exposed resist was developed in a conventional solution of methyl isobutyl ketone–isopropyl alcohol (MIBK-IPA) (1:3) for 30 s. To complete the development process and to avoid PMMA scum, the substrate was immersed for 30s in IPA. Using physical vapour deposition (evaporation rate of 0.3 Å s^{-1}), 5 nm Ti as the adhesion layer, and 45 nm Au were deposited on the sample. The unexposed resist was then removed with acetone and rinsed in IPA. O_2 plasma etching (at 100W for 180s) was used to remove residual resist and organic contaminants. The result is shown in Figure 3 and confirms the feasibility of the NC-PtMM geometry, even though further adjustments are required to reproduce the exact geometry numerically simulated and illustrated in the previous sections (presently, the fabricated crosses show an in-phase organization, whereas a line-to-line out-of-phase fabrication is required, as shown in Figure 1). For practical applications, it is also important to notice that large arrays can be fabricated (in Figure 3, around 150 crosses are shown, even though the actual fabricated number is over 10,000 crosses).

These results demonstrate that the NC-PtMM structure could be fabricated following standard solutions typical of the semiconductor industry, and employed as a top surface coating on TEGs for strongly enhancing their thermal gradient, an essential condition for improved current generations.

Nanoscribe fabrication route

Nanoscribe to make a polymer master, then replicate by NIL

1. Design unit cell as GWL/STL. Use a writing field that covers the intended master area.

2. Print master using IP-DIP or IP-S on a fused silica or silicon substrate. Feature size: Nanoscribe reliably creates features down to ~200 nm; targeting 60 nm arms is challenging and will require an optimised high-NA objective and conservative throughput.
3. Post-develop the master and perform a short oxygen plasma to remove residue.
4. Use the polymer master for PDMS or h-PDMS molding to create NIL stamps, then use thermal or UV-NIL to transfer the pattern to a resist on the final substrate. Metallize the imprinted resist to form the resonators (Cr deposition) then lift-off or etch back as needed.
1. Add ALD Al_2O_3 passivation[21–24].

Direct Nanoscribe + conformal metallization (alternative)

1. Print the Nanocross geometry directly in IP-DIP on a conductive substrate.
2. Metallize the polymer with sputtered Cr (adhesion) + Ag or thick Cr. Use ALD to deposit thin Al_2O_3 encapsulation to improve thermal/radiation stability[21–24].
3. Limitations: polymer backbone may degrade under Space conditions (TID, AO) unless fully encapsulated with inorganic films; adhesion, metal film continuity on polymer, and thermal stability at high hot-side temperatures are concerns.

Practical issues and mitigations

- **Feature size & throughput:** Nanoscribe is slow and limited in area; use it for masters only (route A).
- **Polymer stability:** For Space applications, avoid leaving polymer exposed — use ALD encapsulation or convert master to NIL stamps.
- **Metallization uniformity:** conformal coating into high-aspect trenches is nontrivial; ALD metallization is possible, but metal ALD for Cr/Ag is less developed — sputter/evaporation on a replicated resist may be simpler.

Coupled EM/thermal simulation recipe

The simulations were performed through commercial software COMSOL Multiphysics, which is based on FEM. The optical constants for calculations were measured, and standard optical constants (Palik & Johnson–Christy) for Cr, Au, Ag, Al, and Ni. Dielectric n,k for Al_2O_3 and SiO_2 were obtained from ellipsometry and confirmed with literature. For the electromagnetic solver in frequency-domain sweep mode, we employed RF / Electromagnetics (Frequency Domain) and Wave Optics modules, supplementing each other. As the domain, we used a single unit cell with periodic boundary conditions on lateral faces, and ports (or perfectly matched layers) on top/bottom for normal incidence. Excitation was a normal incidence plane wave. For broadband AM0, we run a dense frequency sweep (e.g., 300–2500 nm, step 5–10 nm), supported by a focus on resonance bands and computed spectral integrals. Maximum element size of the mesh was $\leq \lambda/10$ inside dielectrics and metals for high accuracy; refine to $\leq \lambda/20$ inside thin layers and near metal corners. A boundary layer mesh for thin metal films was employed where required. Outputs were a complex E-field $E(\lambda, r)$ and induced current density $J(\lambda,r)$; computed volumetric heating $Q(r,\lambda) = \frac{1}{2}R\{J \cdot E^*\}$. Spatial maps were saved at selected λ (resonance $\lambda \pm$ offset). For the temporal coupling, we computed spectrally-resolved absorbed power density $Q(r,\lambda)$, integrated over the simulation wavelengths weighted by the AM0 spectral irradiance $I_{AM0}(\lambda)$ to obtain a spectrally-averaged volumetric heating $Q(r)$(units

$W \cdot m^{-3}$) for steady illumination. To simulate pulses, we applied an explicit temporal envelope $f(t)$ – rectangular pulses of width P_{width} and period P_{period}, so that $Q(r,t) = Q(r) \times f(t)$. For time-dependent thermal solving, Heat Transfer in Solids coupled to the volumetric heat source $Q(r,t)$ was employed. We reused refined EM mesh in the top layers where Q is non-uniform, and coarsened in the substrate, but ensured gradient resolution near interfaces. For the boundary conditions, thermal convection/radiation was set to zero for a vacuum (i.e., space around). For time stepping, we used $dt \leq P_{width}/50$ (for 20 ns pulses, $dt \leq 0.4$ ns) for accurate capture of the heating front, and simulated for multiple pulse periods to capture accumulation. Field localisation and T map are presented in the main text (Figure 5).

Table S3. Steady-state temperature rise scaling under continuous illumination
$\Delta T \approx Q_{abs} \times R_{th}$ with $I_{AM0} = 1361$ W/m^2, $A_{eff} = 0.95$. Values in K.

R_{th} (K·m^2·W^{-1})	$C = 1$	$C = 10$	$C = 100$
1×10^{-6}	0.00129	0.01290	0.12900
1×10^{-5}	0.01290	0.12900	1.29000
1×10^{-4}	0.12900	1.29000	12.9000
1×10^{-3}	1.29000	12.9000	129.000

R_{th} represents the effective thermal resistance from the heated PtMM region to the cold sink (including interface and thermal isolation design); optical concentration factor C scales absorbed flux linearly.

0-deg/90-deg absorptance comparison of the NC-PtMM

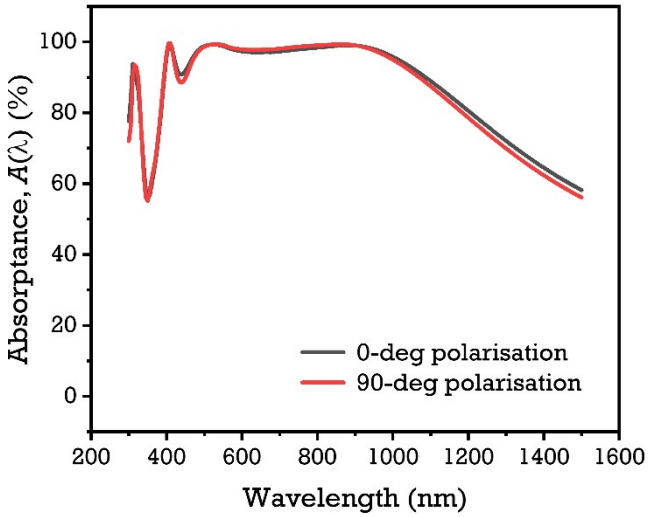

Fig. S1. Absorptance of NC-PtMM at 0-deg and 90-deg polarisation.

References

1 D. K. Oh, T. Lee, B. Ko, T. Badloe, J. G. Ok and J. Rho, Nanoimprint lithography for high-throughput fabrication of metasurfaces, *Front. Optoelectron.*, 2021, **14**, 229–251.

2 N. Mou, X. Liu, T. Wei, H. Dong, Q. He, L. Zhou, Y. Zhang, L. Zhang and S. Sun, Large-scale, low-cost, broadband and tunable perfect optical absorber based on phase-change material, *Nanoscale*, 2020, **12**, 5374–5379.

3 J. G. Ok, H. Seok Youn, M. Kyu Kwak, K.-T. Lee, Y. Jae Shin, L. Jay Guo, A. Greenwald and Y. Liu, Continuous and scalable fabrication of flexible metamaterial films via roll-to-roll nanoimprint process for broadband plasmonic infrared filters, *Applied Physics Letters*, 2012, **101**. DOI: 10.1063/1.4767995.
4 C. Wu, B. Neuner, G. Shvets, J. John, A. Milder, B. Zollars and S. Savoy, Large-area wide-angle spectrally selective plasmonic absorber, *Phys. Rev. B*, 2011, **84**. DOI: 10.1103/PhysRevB.84.075102.
5 B. A. Banks, S. K. Rutledge, J. A. Brady and J. E. Merrow, Atomic oxygen effects on materials, *NASA, Langley Research Center, NASA(SDIO Space Environmental Effects on Materials Workshop, Part 1*, 1989.
6 K. K. de Groh and B. A. Banks, *Atomic Oxygen Erosion Data from the MISSE 2-8 Missions* NASA/TM—2019-219982, 2019, https://ntrs.nasa.gov/citations/20190025445.
7 European Cooperation for Space Standardization (ECSS), *ECSS-Q-ST-70-04C: Thermal testing for the evaluation of space materials, processes, mechanical parts and assemblies*, ECSS Secretariat (ESA-ESTEC), Noordwijk, Netherlands, 2008.
8 D. Wernham and A. Piegari, in *Optical Thin Films and Coatings*, Elsevier, 2018, pp. 789–811.
9 A. Doan, Synergistic Effects of Atomic Oxygen and Ultraviolet Radiation Exposure on Various Spacecraft Materials, *Aerospace Engineering*, 2013.
10 J. A. Dever, A. J. Pietromica, T. J. Stueber, E. A. Sechkar and R. K. Messer, *Simulated Space Vacuum Ultraviolet (VUV) Exposure Testing for Polymer Films*, 39th Aerospace Sciences Meeting and Exhibit AIAA Paper 2001-1054, 2002, https://ntrs.nasa.gov/citations/20020039136.
11 J. Kuhnhenn, M. Steffens and M. Baum, in *International Conference on Space Optics — ICSO 2018*, ed. N. Karafolas, Z. Sodnik and B. Cugny, SPIE, 2018 - 2018, p. 164.
12 K. FUJITA, K. SUZUKI, S. MOTOKOSHI and K. KISARA, Proton Irradiation Effects on Dielectric Coatings on Optics, *Trans. JSASS Space Tech. Japan*, 2009, **7**, Pc_99-Pc_104.
13 European Cooperation for Space Standardization (ECSS), *ECSS-Q-ST-60-15C Rev.1: Space product assurance - Radiation hardness assurance - EEE components*, ECSS Secretariat (ESA-ESTEC), Noordwijk, Netherlands, 2024.
14 M. W. Crofton, D. T. Schoeffler, J. A. Young and M. J. Patterson, Erosion Rate Measurements for DART Spacecraft Ion Propulsion System, *Applied Sciences*, 2022, **12**, 7831.
15 R. Behrisch and K. Wittmaack, *Sputtering by Particle Bombardment III*, Springer Berlin Heidelberg, Berlin, Heidelberg, 1991.
16 Y. YAMAMURA and H. TAWARA, ENERGY DEPENDENCE OF ION-INDUCED SPUTTERING YIELDS FROM MONATOMIC SOLIDS AT NORMAL INCIDENCE, *Atomic Data and Nuclear Data Tables*, 1996, **62**, 149–253.
17 E21 Committee, *Test Method for Total Mass Loss and Collected Volatile Condensable Materials from Outgassing in a Vacuum Environment*, ASTM International, West Conshohocken, PA.
18 European Cooperation for Space Standardization (ECSS), *ECSS-E-ST-10-03C Rev.1: Testing, ECSS Secretariat (ESA-ESTEC)*, Noordwijk, Netherlands, 2022.
19 NASA, *NASA-STD-7001B: Payload Vibroacoustic Test Criteria*, NASA OCE, 2017.
20 NASA Goddard Space Flight Center, *GSFC-STD-7000B: General Environmental Verification Standard (GEVS) for GSFC Flight Programs and Projects*, Greenbelt, MD, USA, 2021.

21 T. Hirvikorpi, M. Vähä-Nissi, A. Harlin and M. Karppinen, Comparison of some coating techniques to fabricate barrier layers on packaging materials, *Thin Solid Films*, 2010, **518**, 5463–5466.
22 D. Jiang, D. Wang, G. Liu and Q. Wei, Atomic Oxygen Adaptability of Flexible Kapton/Al2O3 Composite Thin Films Prepared by Ion Exchange Method, *Coatings*, 2019, **9**, 624.
23 C. Yan, J. Li, Y. Dai, Z. Lan, H. Wang, H. Tong, X. Ye, X. Yuan, C. Liu and H. Li, Fabrication of high-performance ALD-Al2O3/SiO2 nanolaminate coating for atomic oxygen erosion resistance on polyimide, *Surface and Coatings Technology*, 2025, **502**, 131960.
24 T. K. Minton, B. Wu, J. Zhang, N. F. Lindholm, A. I. Abdulagatov, J. O'Patchen, S. M. George and M. D. Groner, Protecting polymers in space with atomic layer deposition coatings, *ACS applied materials & interfaces*, 2010, **2**, 2515–2520.